DUDLEY KNOX LIBRARY
NAVAL POSTGRADUATE SCHOOL
MONTEREY CA 93943-5101

Approved for public release; distribution is unlimited.

Modification of the Naval Postgraduate School Lidar System

by

Gary Mallo
Lieutenant Commander, United States Navy
B.S., University of Oklahoma, 1978

Submitted in partial fulfillment of the
requirements for the degree of

MASTER OF SCIENCE IN SYSTEMS ENGINEERING

From the

NAVAL POSTGRADUATE SCHOOL
September 1994

REPORT DOCUMENTATION PAGE

Form Approved
OMB No. 0704-0188

Public reporting burden for this collection of information is estimated to average 1 hour per response, including the time for reviewing instructions, searching existing data sources, gathering and maintaining the data needed, and completing and reviewing the collection of information. Send comments regarding this burden estimate or any other aspect of this collection of information, including suggestions for reducing this burden, to Washington Headquarters Services, Directorate for Information Operations and Reports, 1215 Jefferson Davis Highway, Suite 1204, Arlington, VA 22202-4302, and to the Office of Management and Budget, Paperwork Reduction Project (0704-0188), Washington, DC 20503

1. AGENCY USE ONLY (Leave blank)	2. REPORT DATE	3. REPORT TYPE AND DATES COVERED
	September 1994	Master's Thesis

4. TITLE AND SUBTITLE MODIFICATION OF THE NAVAL POSTGRADUATE SCHOOL LIDAR SYSTEM

5. FUNDING NUMBERS

6. AUTHOR(S)

MALLO GARY OWEN

7. PERFORMING ORGANIZATION NAME(S) AND ADDRESS(ES)

Naval Postgraduate School
Monterey, CA 93943-5000

8. PERFORMING ORGANIZATION REPORT NUMBER

9. SPONSORING/MONITORING AGENCY NAME(S) AND ADDRESS(ES)

Naval Sea Systems Command
Department of the Navy, Attention PMS-400B
Washington, DC 20363

10. SPONSORING/MONITORING AGENCY REPORT NUMBER

11. SUPPLEMENTARY NOTES

The views expressed in this thesis are those of the author and do not reflect the official policy or position of the Department of Defense or the US Government.

12a. DISTRIBUTION/AVAILABILITY STATEMENT

Approved for public release; distribution is unlimited.

12b. DISTRIBUTION CODE

13. ABSTRACT *(Maximum 200 words)*

The Naval Postgraduate School (NPS) Lidar System was modified to allow comparison of lidar profiles with radiosonde profiles preparatory to evaluation of the lidar as a monitor for changes in the boundary layer. The detector package was modified to permit day and night operation and to reduce the overlap-limited minimum measurement range. Redesign of the transmitter beam expansion optics raised the power threshold for internal optics damage while improving the filling of the 18" output mirror and maintaining eye safe operation. Tests of the system on completion of modification demonstrated clear-air returns to ranges of 1 to 1.5 kilometers. Direct comparison of clear-air lidar returns with radiosonde balloon launches can now be undertaken to evaluate correlation of changes.

14. SUBJECT TERMS	15. NUMBER OF PAGES
lidar, Nd:YAG, radiosonde, laser,lidar profile.	54
	16. PRICE CODE

17. SECURITY CLASSIFICATION OF REPORT	18. SECURITY CLASSIFICATION OF THIS PAGE	19. SECURITY CLASSIFICATION OF ABSTRACT	20. LIMITATION OF ABSTRACT
UNCLASSIFIED	UNCLASSIFIED	UNCLASSIFIED	UL

ABSTRACT

The Naval Postgraduate School (NPS) Lidar System was modified to allow comparison of lidar profiles with radiosonde profiles preparatory to evaluation of the lidar as a monitor for changes in the boundary layer. The detector package was modified to permit day and night operation and to reduce the overlap-limited minimum measurement range. Redesign of the transmitter beam expansion optics raised the power threshold for internal optics damage while improving the filling of the 18" output mirror and maintaining eye safe operation. Tests of the system on completion of modification demonstrated clear-air returns to ranges of 1 to 1.5 kilometers. Direct comparison of clear-air lidar returns with radiosonde balloon launches can now be undertaken to evaluate correlation of changes.

1R278256
c.1

TABLE OF CONTENTS

I. INTRODUCTION 1
A. BACKGROUND 1
B. RESEARCH OBJECTIVES 2
C. LIDAR SYSTEM DESIGN OVERVIEW 2
II. LIDAR THEORY 4
A. INTRODUCTION 4
B. LIDAR EQUATION 4
C. RECEIVER THEORY 9
1. Daytime Lidar Range Determination 12
2. Night Time Lidar Range Determination 13
D. RADAR PROPAGATION IN THE ATMOSPHERE 15
III. LIDAR SYSTEM DESIGN 17
A. OVERALL DESIGN 17
B. LIDAR TRANSMITTER 17
1. Laser 17
2. Dall-Kirkham Telescope 19
3. Laser Optics 20
C. LASER SAFETY 24
D. LIDAR RECEIVER 28
E. DATA ACQUISITION 31
IV. DATA COLLECTION AND ANALYSIS 35
A. SYSTEM DEMONSTRATION 35
B. RANGE LIMITS 35
V. CONCLUSIONS AND RECOMENDATIONS 42
LIST OF REFERENCES 44
INITIAL DISTRIBUTION LIST 46

DUDLEY KNOX LIBRARY
NAVAL POSTGRADUATE SCHOOL
MONTEREY CA 93943-5101

ACKNOWLEDGEMENT

The research reported in this thesis was supported by the Johns Hopkins University/Applied Physics Laboratory, under contract No. 605976-0, and AEGIS Program Office PMS-400B, under document No. N-0002494WRA-0614. A number of people have helped to make this thesis a success. I wish to thank Mike Thomas and his group at APL for their support during my experience tour, Mr. William Lentz for his invaluable assistance due to his previous work in the lidar field, and my thesis advisor, Professor A.W. Cooper, for his support. Finally and most importantly, I want to thank my wife, Paula, for her encouragement and never-ending support.

I. INTRODUCTION

A. BACKGROUND

A lidar system was designed and built at Naval Postgraduate School, Monterey California, to provide range information to atmospheric features such as clouds. It was originally intended to be integrated into the Naval Postgraduate School's Infrared Search and Target Designation system (NPS-IRSTD). The lidar system consisted of a laser transmitter, employing a frequency-doubled Nd:YAG laser, a telescope to expand the beam in order to meet laser safety requirements, and a receiver employing a photomultiplier tube [Ref. 1]. For this thesis it was initially intended to use the Naval Postgraduate School (NPS) lidar to make a comparison with radiosonde balloon atmosphere profiles to determine if the lidar system could be used to monitor changes in the atmospheric vertical profile. The system could then be used as a cuing device to indicate when a new radiosonde launch is required to maintain an accurate radar coverage prediction.

The lidar system was noted to have the following problems that were required to be corrected prior to its use:

1. The detector was limited to night time operation due to high background noise.
2. The laser transmitter was burning the mirrors used to direct the beam to the telescope.
3. The trigger signal was inconsistent.
4. The receiver sensitivity was not adequate for clear air lidar signals.
5. The field of view was too small for near field returns.
6. The detector noise was too high to detect weak signals.
7. A ground loop problem between the transmitter and the receiver existed.
8. A power supply was needed to supply plus and minus five volts, plus and minus six volts, plus twelve volts, and minus eighteen volts to the detector.

B. RESEARCH OBJECTIVES

Due to the number of problems with the lidar system the objective of this thesis was changed from comparison of the lidar profiles to radiosonde balloon data and for its use as a cuing device to the design modification of the Naval Postgraduate School Lidar system to enable it to see clear air lidar signals out to a range of 1-2 kilometers during daytime operation and to eliminate the noted problems.

After the system is modified and at a later date it is intended to perform the comparison to balloons and test the feasibility of a lidar system to be used as a cuing device for launches. The system's initial design requirements to be able to range to clouds will be maintained in the modified system.

The system will be required to meet the laser safety requirements for eye safety. Use of a system that is not eye safe is not allowed for obvious reasons.

C. LIDAR SYSTEM DESIGN OVERVIEW

The modifications to the existing lidar system were limited to those needed to make the system operational for the purpose of measuring clear air returns. Other applications may be desired and added at some time in the future.

The overall system will remain basically the same as it will use the frequency-doubled Nd:YAG laser in the transmitter and the beam will be expanded to an 18 inch diameter for eye safety purposes. The laser safety calculations are detailed in Chapter III. The receiver consists of a telescope to collect the backscattered laser signal and associated optics to filter background noise and focus the signal onto a photomultiplier tube. The receiver design is covered in detail in Chapter III. The data collection was performed using a digital oscilloscope and stored on a floppy disk for off-line analysis. The oscilloscope is accurate enough to allow the determination as to whether or not a lidar signal is present.

This thesis is organized as follows:

1. Chapter II is an Introduction to Lidar Theory and the atmospheric parameters that affect radar propagation.
2. Chapter III is the Design of the Lidar System including laser safety requirements.
3. Chapter IV is Data Collection and Analysis.
4. Chapter V is Conclusions and Recommendations.

II. LIDAR THEORY

A. INTRODUCTION

The use of lidar systems for monitoring the atmosphere is not a new idea. It has been looked at in great detail and should someday be able to provide the same data that currently is only available from radiosonde balloons. The two primary methods being considered for determining the water vapor and temperature profiles are: [Ref. 2]

1. Raman scattering, and
2. differential absorption.

The basic lidar system is made up of three sections. The first is the transmitter section which includes the laser and the associated optics to direct the laser energy in the desired direction. The second is the receiver section which includes the light gathering optics, detector and amplifiers. The third is the data processing section which includes an oscilloscope and a computer for signal analysis.

This thesis is concerned with the use of an aerosol lidar as a cuing device to indicate when a radiosonde launch is needed; the theory of how basic lidar systems work will be covered in detail in the following sections.

B. LIDAR EQUATION

The amount of energy arriving at the detector is dependent upon the initial laser energy transmitted, the probability that the light will be reflected back toward the detector, and the probability that the reflected light will strike the detector. The basic lidar equation that describes these factors is given as: [Ref. 3]

$$Pr = P_0 \frac{A}{R^2} \xi(\lambda) \xi(R) \beta(\lambda, R) \frac{(c\tau)}{2} e^{-2\int_0^R \kappa(R)\, dR} \qquad 2\text{-}1$$

where

P_r is the energy received by the detector;

P_0 is the initial energy transmitted by the laser;

A_0 is the effective aperture of the receiver optics;

R is the range from the detector defined as $c\Delta t/2$;

$\xi(\lambda)$ is the transmission efficiency of the receiver optics at wavelength λ;

$\xi(R)$ is the geometric form factor ;

$\beta(\lambda,R)$ is the backscatter coefficient at R and wavelength λ;

c is the speed of light;

τ is the laser pulse width;

$\kappa(\lambda)$ is the attenuation coefficient of the atmosphere for wavelength λ.

Since the wavelength of the laser and the detector system are the same for a monochromatic aerosol lidar the wavelength dependance will be omitted from the lidar equation for the rest of this report.

The transmission efficiency factor $\xi(\lambda)$ is a constant value which is only dependant on the lenses and filters used in the receiver. The geometric form factor $\xi(R)$ is comprised of two factors. The first is the overlap function which is broken up into three categories for a biaxial lidar system. The second is the effect due to the reflected lidar signal from the near field not being in the focal plane of the receiver telescope. This results in the received signal increasing as range is increased and the image plane moves to the focal plane for an object at infinity. The signal has a $1/R^2$ dependence but because of the geometric effect previously discussed the actual lidar signal increases until the range reaches a value at which most of the irradiance of the backscattered lidar signal is focused onto the detector. At this point the lidar signal will decrease as $1/R^2$. The three categories of the overlap function are (a) no overlap, (b) complete overlap, and (c) partial overlap (see Figure 1). The first two can be easily handled but the third is a difficult problem. [Ref.4]

Both components of the geometric form factor are dependent on the system configuration or geometry and do not vary with each laser firing. Since a change in

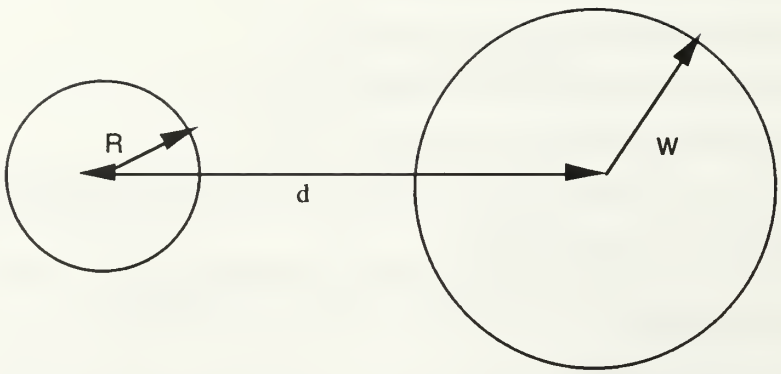

a) No Overlap

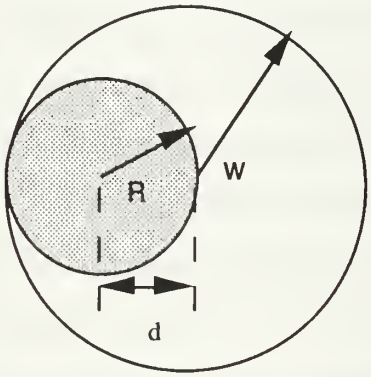

b) Complete Overlap

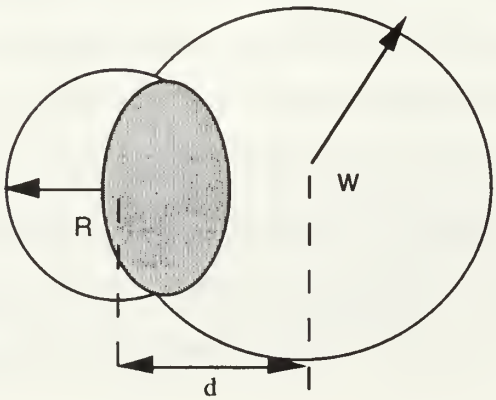

c) Partial Overlap

Figure 1. Three overlap situations possible for a biaxial lidar. R is the radius of the laser illumination, W the radius of the receiver field of view, d is the axis spacing.

the atmospheric conditions is the factor of concern, the geometric factors cancel out when comparing the change from one profile to the next. This allows the use of the partial overlap area to indicate a change in atmospheric factors even though the actual parameters themselves would be difficult to measure. The geometry of a basic lidar system would depend on the laser location with respect to the detector. This would include the separation of the receiver and laser axes (d), the laser beam divergence (θ) and the receiver telescope opening angle (ϕ). Figure 2 shows the basic geometry of a biaxial lidar system. [Ref. 3]

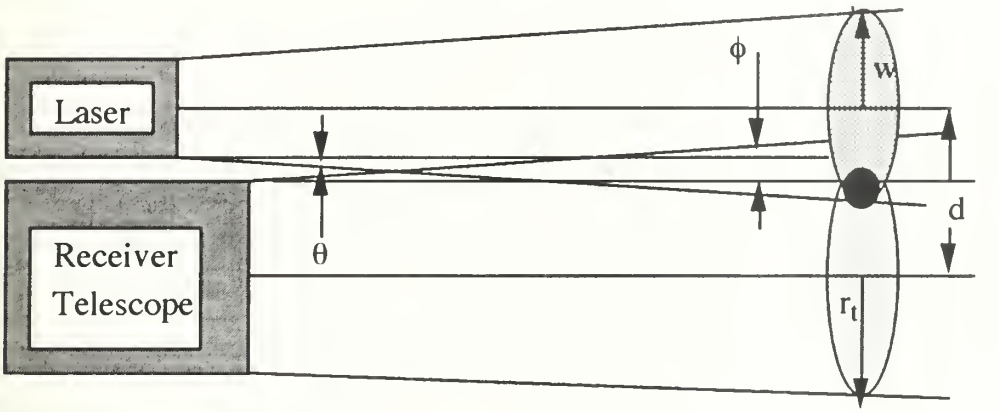

Figure 2. Geometry of a Biaxial Lidar System. W is the radius of the laser circle of illumination and r_t is the radius of the circular field of view.

The next term in the lidar equation is the atmospheric volume backscatter coefficient $\beta(\lambda,R)$. $\beta(\lambda,R)$ is the backscattered intensity per unit solid angle per unit path length (kilometers^{-1} steradian^{-1}). $\beta(\lambda,R)$ can be expressed as

$$\beta(\lambda, R) = \frac{N(R)\,\sigma^s(\lambda)}{4\pi} \qquad 2\text{-}2$$

where N(R) is the number density of the species at range R responsible for the backscattered radiation at wavelength λ and $\sigma^s(\lambda)$ is the relative cross section. Since $\sigma^s(\lambda)$ is a constant, the variation in $\beta(\lambda,R)$ is due to the number density change. For

maritime areas the primary aerosol is water vapor which varies as a function of altitude. It is this parameter that can be used to indicate a change in the relative humidity. And again since it is only a change that is to be detected to indicate whether or not a new radiosonde launch is needed, the change in the lidar signal would be an indication of a change in $\beta(\lambda,R)$, which would be an indication of a change in the relative humidity.

The next term in the lidar equation is the transmission factor which can be expressed as:

$$T(\lambda, R) = -2\int_{r_0}^{r} \kappa(\lambda, R)\, dR \qquad 2\text{-}3$$

Where $\kappa(\lambda,R)$ is the extinction coefficient as a function of wavelength and range. The wavelength is constant, but the extinction coefficient varies due to variation in the number of absorbers and scattering molecules as the range changes. The extinction coefficient can be further reduced to

$$\kappa(\lambda, R) = \sigma^{a}(\lambda, R) + B(R, \lambda, \theta) \qquad 2\text{-}4$$

Where

$\sigma^{a}(\lambda,R)$ is the atmospheric absorption coefficient, and
$B(\lambda,R,\theta)$ is the atmospheric scattering coefficient from which $\beta(\lambda,R)$ is derived.

The wavelength dependence in equation 2-4 will be omitted due to the use of a monochromatic laser. The $\sigma^{a}(R)$ term is the sum of the aerosol and molecular (Mie and Rayleigh) scattering coefficients. The dominant absorbers and scatterers depend on the frequency of the light propagating through the atmosphere. The range dependence is due to the variation in the number density of the absorbers and scatterers along the path of the laser beam.

C. RECEIVER THEORY

In order for the lidar system to provide useful information the receiver section must be able to detect the backscattered laser signal against the background noise. This section will describe photomultiplier tube, pre-amplifier, and logarithmic amplifier operation.

The photomultiplier tube is a vacuum tube photoemissive detector consisting of photocathode, some number of dynodes, and an anode as shown in Figure 3. When photons of sufficient energy strike the cathode free electrons are generated. The electrons are accelerated towards the anode by an electric field and dynodes are placed such that as the electrons move toward the anode they strike the first of a chain of dynodes. The dynodes are maintained at a high potential and for each electron that strikes the dynode δ secondary electrons are generated. These secondary electrons then strike the next dynode in the chain, generating more electrons. The total gain is dependent on the number of dynodes, the material used and the potential between dynodes. The gain can be described as $G=\delta^N$ where N is the total number of dynodes.[Ref. 5]

Some disadvantages of using photomultiplier tubes are:

1. High voltage is required to achieve the desired gain.
2. The wavelengths are restricted to the visible and ultraviolet spectrum.
3. The tubes are fragile.
4. The quantum efficiencies are generally low (10-25%).

The advantages of the photomultiplier tube are:

1. High gains which allow detection of very weak signals.
2. Low internal noise.
3. High signal gain to noise gain ratio,
4. Large detector area,
5. Fast response times, typically on the order of 2 nanoseconds.

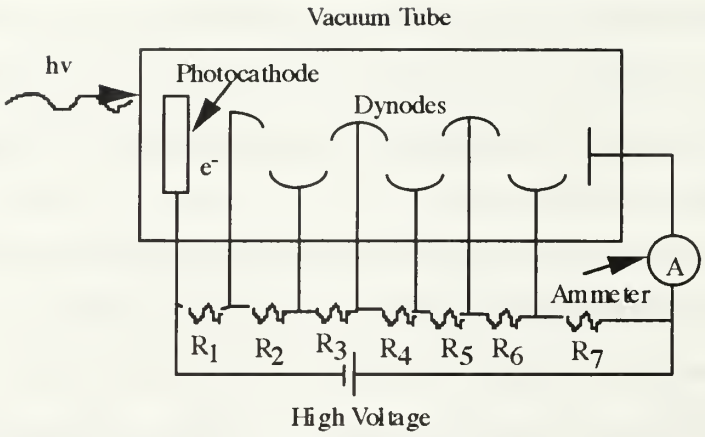

Figure 3. Photomultiplier tube block diagram [Ref. 5].

There are four types of noise that must be considered when describing detector systems. These are:

1. Shot noise (i_N). This noise is the result of the statistical generation of electrons by the cathode. The rms value of the shot noise current is given as [Ref.6]:

$$i_N = \sqrt{2e\,(i_s + i_d + i_b)\,\Delta f G^2} \qquad 2\text{-}5$$

where
i_s is the current on the cathode from the lidar backscattered signal,
i_d is the dark current (the thermally generated current in the absence of any light),
i_b is the current generated by the background light,
e is the electron charge,
Δf is the system bandwidth,
G is the gain of the photomultiplier.

2. Johnson or thermal noise (i_j). This is the noise generated from the thermal excitation in a resistor. The rms value of the Johnson noise can be written as [Refs. 6 and 7]:

$$i_{Jrms} = \sqrt{\frac{4kT\Delta f}{R}} \qquad 2\text{-}6$$

where R is the equivalent resistance of the photomultiplier and load.

3. Background noise (i_b). This is the noise component which results from the radiant spectral energy from the sun. Since this noise is the limiting source of

noise during daytime operation of photomultiplier tube detectors it will be fully discussed here. The background noise level can be reduced by matching the field of view of the detector to that of the transmitted laser field of view as closely as possibly and by the use of a narrow band filter. The background current can be written as [Refs. 6 and 7]:

$$\overline{i_b} = \frac{\lambda e \eta(\lambda) E_b(\lambda)}{hc\tau_d} \qquad 2\text{-}7$$

where

λ is the wavelength of the background radiation,
$\eta(\lambda)$ is the quantum efficiency of the photomultiplier tube,
$E_b(\lambda)$ is the background spectral energy,
e is the electron charge,
c is the speed of light,
h is Plank's constant, and
τ_d is the detection interval, which is not the same as the laser pulse width.

Assuming that the terms that describe the background energy ($E_b(\lambda)$, which is dependent on the wavelength) are constant over the bandwidth of the optical filter, $E_b(\lambda)$, can be written as:

$$E_b(\lambda) = \Delta\lambda S_b(\lambda)\tau_0(\lambda)\Omega_0 A_0 \tau_d \qquad 2\text{-}8$$

where

$\Delta\lambda$ is the narrowband filter wavelength interval,
$S_b(\lambda)$ is the background spectral radiance,
$\tau_0(\lambda)$ is the transmittance efficiency of the receiver optics,
Ω_0 is the receiver solid angle,
A_0 is the receiver's effective aperture, and
τ_d is the detection interval.

Substituting equation 2-8 into equation 2-7 yields the following:

$$\overline{i_b} = \frac{\lambda e \eta(\lambda) \Delta\lambda S_b(\lambda)\tau_0(\lambda)\Omega_0 A_0}{hc} \qquad 2\text{-}9$$

4. Quantum noise. This noise is generated from the statistical fluctuations in the generation of the secondary electrons at the dynodes in the photomultiplier tube. When the gain of the first dynode in the chain is high, the dynode noise is negligible and can be neglected. [Ref. 6]

The signal-to-noise ratio (SNR) can be written, from equations 2-5 and 2-6, as: [Refs. 6 and 7]

$$SNR = \frac{i_s^2 G^2}{(2e(\overline{i_s} + \overline{i_b} + \overline{i_d})\Delta f G^2 + \frac{4kT\Delta f}{R})} \quad . \qquad 2\text{-}10$$

When R is large enough the Johnson noise is small compared to the shot noise term and can be neglected. The two cases left to consider are daytime and night time. These will be discussed in detail since they determine the maximum range of the lidar system.

1. Daytime Lidar Range Determination

When the lidar will be operated during daytime the background noise is the limiting factor and $i_b >> i_s + i_d$. Therefore the SNR equation can be simplified to:

$$SNR = \frac{i_s^2 G^2}{2e\overline{i_b}\Delta f G^2} \qquad 2\text{-}11$$

For single pulses the minimum detectable signal can be found by letting SNR=1. This is the best case situation and is the theoretical minimum. The minimum detectable power can be determined by:

1. Noting that the signal current can be written as a function of the incident power P(r): [Ref. 6]

$$i_s = \frac{\lambda e \eta(\lambda) P(r)}{hc} \qquad 2\text{-}12$$

2. Now substituting equations 2-7 and 2-12 into equation 2-11 and solving for P(r) with SNR = 1 yields:

$$P(r) = \sqrt{\frac{2hc\Delta\lambda S_b(\lambda)\tau_0(\lambda)\Omega_0 A_0 \Delta f}{\lambda\eta(\lambda)}} \qquad 2\text{-}13$$

By solving the lidar equation (2-1) for range (r) and substituting equation 2-13 for P(r) the maximum theoretical daytime range can be written as:

$$r_{max} = \sqrt{\frac{P_0\tau\beta(r)\sqrt{cA_0\lambda\eta(\lambda)}\,exp\left[-2\int_0^{max}\sigma(r')\,dr'\right]}{\sqrt{8h\Delta\lambda S_b(\lambda)\tau_0(\lambda)\Omega_0\Delta f}}} \qquad 2\text{-}14$$

where

r_{max} is the maximum range of the lidar system (meters),
P_0 is the transmitted power (watts),
τ is the laser pulse width (seconds),
$\beta(r)$ is the atmospheric volume backscattering coefficient at range r (meters^{-1} * steradians^{-1}),
c is the speed of light (meters per second),
A_0 is the effective aperture of the receiver (meters^2),
λ is the wavelength of the background radiation which due to the narrow band filter can be assumed to be the same as the laser wavelength (meters),
$\eta(\lambda)$ is the quantum efficiency of the photomultiplier tube,
$\sigma(r)$ is the atmospheric extinction coefficient (meters^{-1}),
h is Plank's constant (watts * seconds^2),
$\Delta\lambda$ is the narrow band filter width (microns),
$S_b(\lambda)$ is the spectral radiance of the background (watts * meters^{-1} * steradians^{-1} * microns^{-1}),
$\tau_0(\lambda)$ is the receiver optics transmission efficiency at wavelength λ,
Ω_0 is the receiver solid angle (steradians), and
Δf is the receiver bandwidth (Hertz).

2. Night Time Lidar Range Determination

During night time operation the signal current i_s is much greater than the background and dark currents which can therefore be neglected. The SNR for night time can then be written as:

$$SNR = \frac{i_s^2 G^2}{2e\bar{i}_s \Delta f G^2} \qquad 2\text{-}15$$

which simplifies to:

$$SNR = \frac{i_s^2}{2e\bar{i}_s \Delta f} \quad . \qquad 2\text{-}16$$

If the photomultiplier rise time is shorter than the laser pulsewidth the signal current i_s is approximately the same as the average i_s value and equation 2-16 can be further simplified to:

$$SNR = \frac{i_s}{2e\Delta f} \qquad 2\text{-}17$$

or

$$SNR = \frac{\lambda e \eta(\lambda) P(r)}{2ehc\Delta f} \quad . \qquad 2\text{-}18$$

Again by letting SNR=1 and solving for P(r) equation 2-18 becomes:

$$P(r) = \frac{2hc\Delta f}{\lambda \eta(\lambda)} \quad . \qquad 2\text{-}19$$

The night time maximum range can be found by substituting equation 2-19 into the basic lidar equation (2-1). The receiver optics transmission efficiency is accounted for by multiplying P(r) by $\tau_0(\lambda)$. The resulting expression for the maximum night time range is given by:

$$r_{max} = \sqrt{\frac{P_0 \tau \beta(r) \tau_0(\lambda) A_0 \lambda \eta(\lambda) exp[-2\int_0^{r_{max}} \sigma(r')\, dr']}{4h\Delta f}} \qquad 2\text{-}20$$

where

r_{max} is the maximum range of the lidar system (meters),
P_0 is the transmitted power (watts),
τ is the laser pulse width (seconds),
$\beta(r)$ is the atmospheric volume backscattering coefficient at range r (meters^{-1} * steradians^{-1}),
A_0 is the effective aperture of the receiver (meters^2),
λ is the wavelength of the background radiation which due to the narrow band filter can be assumed to be the same as the laser wavelength (meters),
$\eta(\lambda)$ is the quantum efficiency of the photomultiplier tube,
$\sigma(r)$ is the atmospheric extinction coefficient (meters^{-1}),
h is Plank's constant (watts * seconds^2),
$\tau_0(\lambda)$ is the receiver optics transmission efficiency at wavelength λ, and
Δf is the receiver bandwidth (Hertz).

The primary reason for deriving the maximum daytime and night time range equations is to provide a means to estimate the capability of the system to meet our objectives for different atmospheric conditions.

D. RADAR PROPAGATION IN THE ATMOSPHERE

When attempting to accurately model the propagation of radar (microwaves) it is required to know the radio refractivity. The radio refractivity (N_{ref}) is described by the following equation: [Ref. 8]

$$N_{ref} = 77.6\frac{P}{T} - 5.6\frac{e}{T} + 3.73 \times 10^5 \frac{e}{T^2} \qquad 2\text{-}21$$

where P[mb] is the total atmospheric pressure, T[K] is the temperature, and e[mb] is the water vapor partial pressure.

Ducts are caused by large changes in humidity and temperature which are typically found in the sea-surface boundary layer. It is these ducts and how they have changed since the previous radiosonde launch that are of particular interest.

Currently radiosonde balloons are used to measure the atmospheric parameters of interest in the calculation of the refractivity index. There is however no method

to verify that the radiosonde data is still valid after a few hours. Since a change in the primary parameter that is measured by the radiosonde (relative humidity) would also result in a change in the lidar return signal [Ref. 9], the lidar system could be used to monitor the atmosphere and indicate when there is a need for a new radiosonde launch.

For a lidar system to be used as discussed above it needs to be able to detect changes in the boundary layer. This requires that the system be able to look vertically approximately 1-1.5 kilometers.

There is a strong interest in the atmospheric marine boundary layer since this is where the atmospheric effect on radar and electro-optical signal propagation is the greatest. It would be a significant tactical advantage to know when the atmospheric conditions have changed enough to significantly degrade the current performance predictions. This Thesis will concentrate on the modification of the NPS Lidar System to allow clear air lidar returns out to a range of 1-1.5 kilometers. Once the system has been modified the comparison of the lidar vertical profiles to the radiosonde balloon profiles can be performed.

III. LIDAR SYSTEM DESIGN

A. OVERALL DESIGN

The initial design was done to achieve the maximum possible range within the constraints of eye safety and the availability of the laser. The initial lidar system consisted of a frequency doubled Nd:YAG medical laser, a 17.75 inch telescope to expand the beam to meet eye safety requirements, a detector containing a photomultiplier tube and associated optics to focus the signal onto the tube, a digital oscilloscope to collect the data and a computer for data storage and off-line analysis. A block diagram of the initial design is shown in Figure 4. Since the system is to be used to monitor the atmosphere near the Naval Postgraduate School grounds and the airspace of the Monterey airport the main constraint is eye safety. [Ref. 1]

The basic overall design will remain basically the same; however the internals of both the receiver and laser transmitters are significantly modified to allow clear lidar returns suitable for the end use of comparison to radiosonde data. The specific design changes will be discussed including the reasons for each.

B. LIDAR TRANSMITTER

1. Laser

The laser used in the transmitter is still the frequency-doubled Nd:YAG laser model MK 100 manufactured by Kigre Incorporated. The laser head and power supply are separate units. The power supply unit contains the control section for the laser. The number of pulses per shot is selected in steps of one from 1 to 5 and the laser output power has eight different selectable settings (see Table 1). A power meter is also part of the power supply unit. Table 1 lists the laser

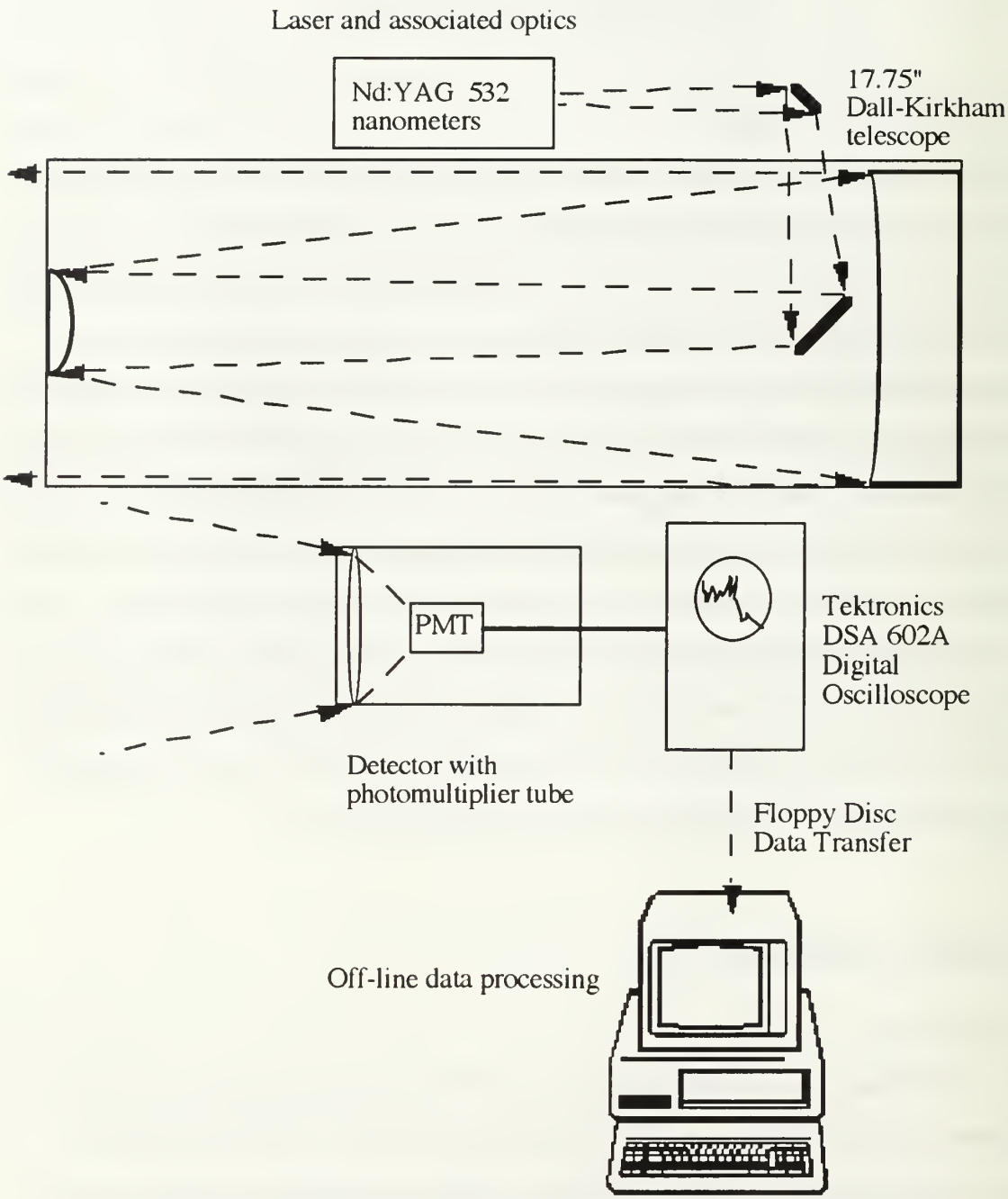

Figure 4. Initial Lidar System Block diagram [Ref. 1].

Table 1: LASER SPECIFICATIONS [REF.1]

Characteristic	Value	Comment
Maximum Energy Output (5 pulses per shot)	mean = 9.126 millijoules σ = 1.587 millijoules	From Table 1 of Ref. 1
Beam Diameter	4.0 $\pm$ 0.2 millimeters	From Table 1 of Ref. 1
Half Angle Beam Divergence	0.165 $\pm$ 0.001 milliradians	From Table 1 of Ref. 1
Energies Available (Single shot only)	Laser Setting / Measured Values .9 / .47 1.2 / .68 1.8 / .65 2.5 / .912 4.0 / .87 5.0 / 1.22 7.5 / 1.36 10.0 / 2.06 All values in millijoules	Measured using an RJ7100 power meter with an RJ736 probe. Note: measurements were taken with the side of the laser box removed. The output energy indicates that the laser should be returned to Kigre Incorporated for repair.

2. Dall-Kirkham Telescope

The telescope was inspected and it was decided that it should still meet the needs for this thesis but should either be replaced or refurbished in the future due to the pitting that was previously noted [Ref.1]. The Dall-Kirkham is a Cassegrain telescope and its specifications are listed in Table 2.

The telescope has a 3.125 inch diagonal mirror to redirect the focal plane 90 degrees back onto the telescope axis. The telescope is mounted on a Pelco PT2000L Pan and Tilt Unit to allow lidar ranging and profiling in azimuth and elevation. The pan and tilt unit can change elevation to $\pm 90^0$ and azimuth 0 to 355^0.

Table 2: DALL-KIRKHAM TELESCOPE SPECIFICATIONS [Ref. 1]

Manufacture	Tinsley Laboratories Incorporated 3900 Lakeside Avenue Richmond, California 94806
Primary Mirror	Diameter: 17.75 inches (aspheric) Radius of Curvature: 126 inches Focal length: 63 inches Optical coating: Al/SiO Substrate: Cervit F number: 3.55
Secondary Mirror	Diameter: 5.75 inches (spherical) Radius of Curvature: 44.8 inches Optical coating: Al/SiO Substrate: Cervit
Overall System	Effective focal length: 159.75 inches Mirror separation: 46.25 inches (vertex to vertex) Effective F number: 9.0 Focal plane is 21 inches behind the vertex of the primary mirror.

3. Laser Optics

The initial transmitter box was configured such that the laser output first went through a beam splitter that directed the 1.06 μm portion of the beam to a beam stop. The beam was then redirected 90° by a mirror, and then the second mirror redirected the beam another 90°. After the beam was redirected by the second mirror it was expanded by a -74mm focal length lens. The expanded beam was then redirected out of the transmitter box onto the 3.125 inch diagonal in the telescope by a mirror attached to a precision mount (see Figure 5).

This design resulted in the first mirror being burned. This problem had to be corrected before the lidar could be used. The first attempt to correct the problem was to install 99.9% reflective mirrors in place of the less reflective ones initially

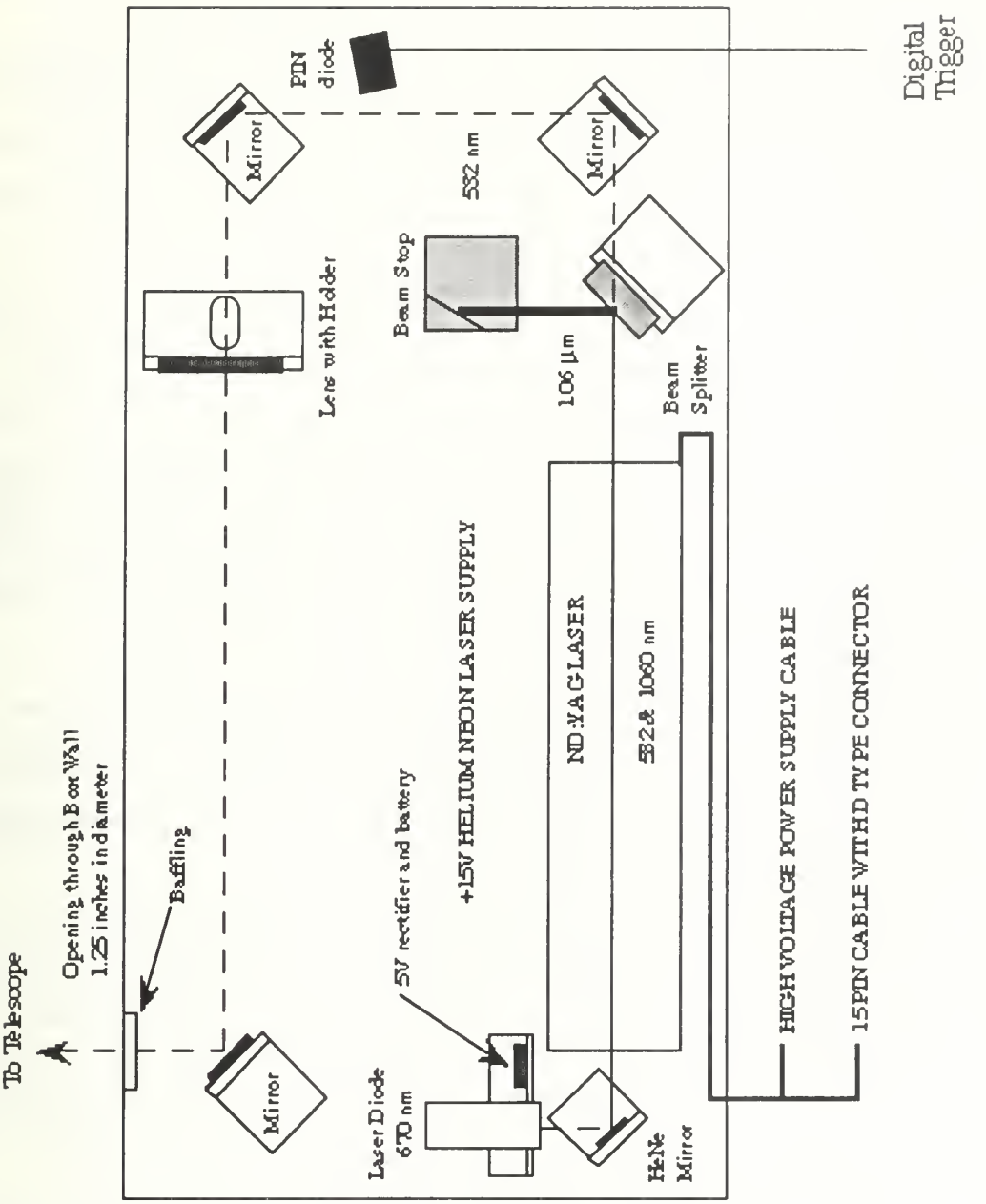

Figure 5. Initial Laser Transmitter Box Design.

used. This did correct the burning problem but then it was noted that the beam was expanding too much before exiting the laser optics box. This was resulting in approximately 40-50% of the laser energy being lost with a significant reduction in the backscattered laser signal. The other problem noted with the transmitter was that

the trigger signal was inconsistent. This needed to be corrected before data could be collected with the oscilloscope.

The laser beam was over-filling the secondary mirror which was further reducing the return signal. Another problem discovered was that the laser box was about 1/4" too far toward the rear of the telescope. This resulted in the output beam not being uniform.

Since several problems existed with the transmitter the decision was made to change the configuration to correct the noted problems and to provide easier alignment of the transmitter.

The first modification was to expand the laser beam before the first mirror. This completely eliminated the possibility of burning any mirrors. Second by using a telescope to control the beam expansion it was significantly easier to set the beam divergence to just fill the secondary mirror.

Next the 45^{o} 532 nanometer reflective mirror was used to redirect the beam through the second lens of the collimating lens set (telescope), see Figure 6, and onto the 3.125" diagonal mirror. This filtered out the 1.06 μm wavelength and reflected 99.9% of the 532 nm wavelength.

The PIN diode was moved out of the laser box. A fiber optic cable was installed to detect the laser pulse off the rear of the laser head and to provide the signal to the PIN diode which was located in a box attached to the end plate of the laser box, see Figure 7. This configuration resulted in a trigger that was not only stable but much larger in strength, ~1-2volts, than the original design. The laser trigger signal ensured that the data collection was triggered on an actual laser pulse vice the laser flashlamp noise.

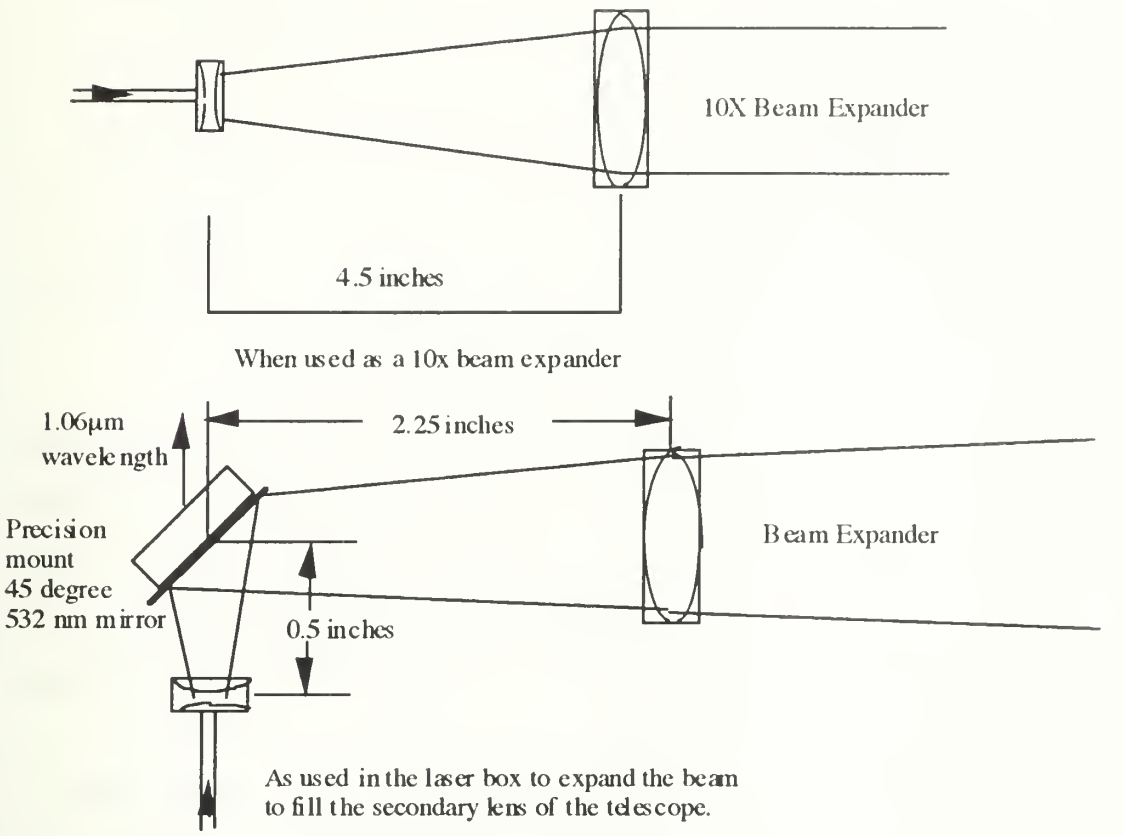

Figure 6. Collimating lens set.

The beam expanding optics were placed to fill the secondary mirror. The radius of the secondary mirror was chosen as the 99% point. The spacing between the first and second lenses of the collimator was calculated in order to provide the required beam expansion taking into account the distance to the focal point. The matrix used to calculate the solution for two lenses is:

$$\begin{bmatrix} w' \\ \theta' \end{bmatrix} = \begin{bmatrix} 1 & T_2 \\ 0 & 1 \end{bmatrix} \begin{bmatrix} 1 & 0 \\ \frac{-1}{f_2} & 1 \end{bmatrix} \begin{bmatrix} 1 & T_1 \\ 0 & 1 \end{bmatrix} \begin{bmatrix} 1 & 0 \\ \frac{-1}{f_1} & 1 \end{bmatrix} \begin{bmatrix} w_0 \\ \theta_0 \end{bmatrix} \qquad 3\text{-}1$$

where

w' is the beam radius on the secondary mirror at the 1/e point (48.68 millimeters),

θ' is the half angle beam divergence required to fill the secondary at the 1/e point and knowing the focal plane location (27.53 milliradians),
T_2 is the distance from the second lens of the collimating set to the secondary mirror (millimeters),
f_2 is the focal length of the second lens of the collimating set (100 millimeters),
T_1 is the distance from the first to the second lens of the collimating set (millimeters),
f_1 is the focal length of the first lens of the collimating set (-12.7 millimeters),
w_0 is the laser beam waist radius (2 millimeters),
θ_0 is the laser beam half angle divergence (0.165milliradians).

The 45° 532 nanometer-reflective dichroic mirror was placed 0.5 inches from the first lens of the collimating set. This prevents the beam from over filling the mirror. The beam diameter is 8 mm (0.315 inches) at the mirror which is 1.25 x 1.75 inches. Also the 3.125 inch diagonal is of sufficient size to redirect the entire beam to the secondary mirror since the beam diameter at the diagonal is 38.78 mm (1.53 inches).

The collimating lens set was adjusted to fill the secondary mirror by monitoring the beam at the secondary mirror. The distance from the first lens of the collimating lens set to the secondary mirror is 151.76 cm. The final half-angle beam divergence out of the Dall-Kirkham telescope was measured and found to be 0.362 milliradians. This would meet the laser safety requirements since the laser beam would never focus in the far field.

C. LASER SAFETY

Laser safety is a major concern in lidar design and operation. The laser beam had to be greatly expanded to meet the requirements for the maximum allowed energy density, the Maximum Permissible Exposure (MPE), of 0.5×10^{-6} joules per centimeter^2 [Ref. 10]. It is assumed for laser safety purposes that 99% of the energy that enters the telescope reaches the secondary mirror. This should be a reasonable

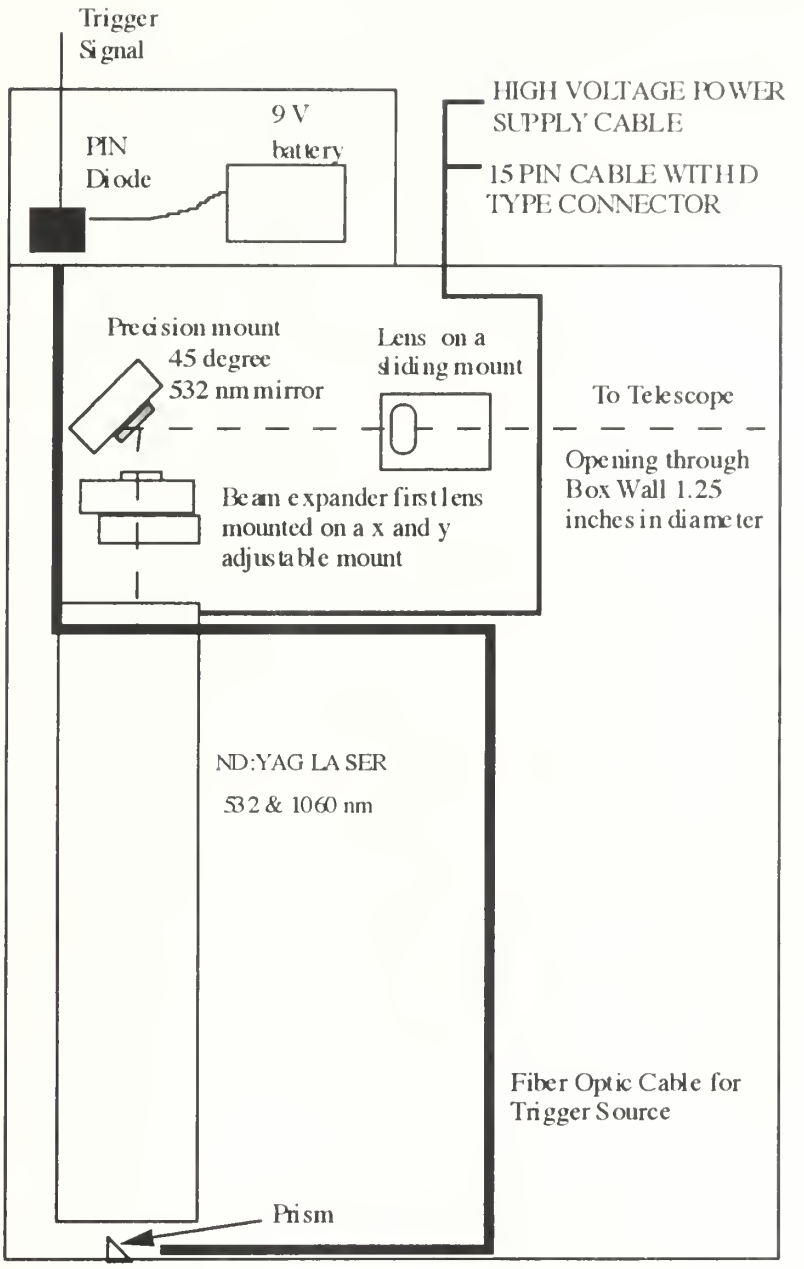

Figure 7. Laser Transmitter Box.

assumption since the beam has been expanded to fill the secondary mirror (see Equation 3-1). The secondary blocks a portion of the beam that exits the telescope and the reduced energy will be accounted for in the laser safety calculations.

The range at which the laser beam can safely be viewed is called the Nominal

Ocular Hazard Distance (NOHD) [Ref.10]. The geometry of the beam, the laser power, and MPE all define the NOHD. The primary means to prevent damage to personnel is to ensure they are either outside the NOHD or wear protective goggles. Table 3 lists the NOHD for all the laser settings. NOHD is calculated using the equation:

$$H = \frac{Qexp[-\mu r]}{\pi\left[\frac{(a+r\phi)}{2}\right]^2} \qquad 3\text{-}2$$

where

H is the radiant exposure (joules per centimeter^{-2}),
Q is the pulsed laser radiant output (joules and defined at the 1/e point),
μ is the atmospheric attenuation coefficient,
r is the range (centimeters),
a is the laser beam diameter at the 1/e point (centimeters),
ϕ is the laser beam divergence angle (milliradians).

The reduction in the output energy will be corrected for in the final calculation of the NOHD for each laser setting. Since the laser beam is Gaussian the fraction of energy blocked by the secondary mirror can be determined by [Ref. 11]:

$$\frac{P_S}{P_T} = 1 - exp\left(\frac{-2D_S^2}{D_L^2}\right) = 0.4045 \qquad 3\text{-}3$$

where

P_S is the power blocked by the secondary mirror,
P_T is the total power of the laser beam,
D_S is the diameter of the secondary mirror (centimeters),
D_L is the diameter of the laser beam at the 1/e point (centimeters).

The denominator of equation 3-2 must be corrected for the area blocked by the secondary mirror also. The denominator can be rewritten as:

$$\pi\left[\frac{(a+r\phi)}{2}\right]^2 = \pi\left[\frac{(D_L+r\phi)}{2}\right]^2 - \pi\left[\frac{D_S}{2}\right]^2 \qquad 3\text{-}4$$

Taking into account that Q in equation 3-2 is the energy contained in the beam between the 1/e points Q can be written as 0.86 X Q_T where Q_T is the total energy in the laser beam [Ref. 11]. Equation 3-2 can now be written as:

$$H = \frac{(1-0.4045)\,0.86Q_T exp[-\mu r]}{\pi\left[\frac{(D_L+r\phi)}{2}\right]^2 - \pi\left[\frac{D_S}{2}\right]^2} \qquad 3\text{-}5$$

where

D_L = 28.7 cm,
H = MPE = 0.5 x 10^{-6} j-cm^{-2}
D_S = 14.61 cm
ϕ = 0.724 x 10^{-3}rad.

The question of what happens to the energy that was blocked by the secondary mirror is one of concern when considering eye safety. Some is reflected back into the transmitter box and some is absorbed by the walls of the inside of the telescope which are painted black. The amount that leaves the telescope is a matter that needs further review. This could be done using a power meter and comparing the output energy with that predicted by the laser safety calculations. The potential eye hazard can then be determined.

Table 3: NOHD

Laser Setting	Laser Energy Measured at the Laser Box Exit Q_T (millijoules)	NOHD (meters) Assuming no atmospheric attenuation
10	2.06	347.4
7.5	1.36	219.2
5.0	1.22	190.3
4.0	0.87	110.7
2.5	0.912	120.9
1.8	0.65	53.5
1.2	0.68	61.7
.9	0.47	0.6

The worst case NOHD is calculated in Table 3 by assuming there is no atmospheric attenuation. The actual NOHD should be less than the values in column 3 of Table 3. The laser output energy for each setting is less than the values for the same setting in Reference 1. This indicates that the laser needs to be sent back to the manufacture for repairs. It was also noted during the firing of the laser that the power would drop and become inconsistent if the laser was fired with less than approximately two seconds between shots. This should not result in a laser safety problem since the energy went down.

D. LIDAR RECEIVER

The original receiver was not usable during daytime due to noise. Its sensitivity had to be improved to allow the monitoring of the boundary layer, which is the final objective of this thesis. A ground loop problem existed between the transmitter and the detector which would result in signal degradation or loss.

It was decided that the detector system should be modified to correct the noted problems. The first step was to replace the lens with a telescope to gather the backscattered light, see Figure 8. A suitable cassegrain telescope was found with a focal length of 750 mm and an F number of 6. The telescope was mounted on top of the receiver box that houses the photomultiplier tube (PMT). To limit any stray light from entering the system the telescope was coupled to the PMT by first redirecting the 532 nm wavelength signal 90° with a 532 nm 45° selective mirror. This would provide the first filter to limit the background light. The 532 nm light is then collimated with an F-3.5 lens to allow the signal to be passed at normal incidence through two 10 nm wide filters centered at 532 nm. The light shield tube and housing for the 45° mirror were painted black to absorb as much stray light as possible and reduce the background noise. The use of a tube prevents light leaks in the box from introducing more background noise. The F-3.5 lens was placed to also focus the signal onto the PMT. To provide the required fine adjustment capability needed to ensure the signal strength is maximized, the 45° mirror assembly was made with vernier control of the left/right and up/down adjustment. This was for the final alignment adjustments after the initial coarse alignment.

The field of view was not restricted with a pinhole since the objective is to look at the boundary layer. This will result in a reduced maximum range to targets such as clouds for daytime operation only. The field of view is 0.5067×10^{-3} steradians or a half angle subtense of 12.7 milliradians. The range at which beam overlap begins is found using Equation 3-6. The range where complete overlap occurs can be found using Equation 3-7.

$$(R + 1)\,\phi + R\theta = 0.0889 \qquad 3\text{-}6$$

$$(R + 1)\,\phi = R\theta + 0.5389 \qquad 3\text{-}7$$

Where

R is the range (meters),
ϕ is the receiver half angle field of view (milliradians),
θ is the laser beam half angle divergence (milliradians).

Solving Equations 3-6 and 3-7, the initial beam overlap starts to occur at a range of 5.9 meters and complete overlap at 42.6 meters (see Figure 9).

The original PMT was determined to be excessively noisy and was replaced with a new R1913. An R928 was considered as a replacement but during testing proved to be less sensitive than the new R1913. The R1913 PMT specifications are listed in Table 4. A LeCroy Model VV100B wideband pulse amplifier was installed in the PMT box and was coupled to the PMT to minimize the capacitance. This was done to reduce the RC time constant as much as possible and at the same time to use a 500 ohm resistor to prevent over-driving the PMT. The amplifier has a gain of 10, a rise time of less than 2 nanoseconds, and a bandwidth of greater than 200 MHz [Ref. 12]. The measured capacitance was 25 pF. This provided a resolution of 12.5 ns or 1.875 m. This should be sufficient for the atmospheric monitoring.

The output of the LeCroy amplifier was AC coupled to an Analog Modules, Model 382 Logarithmic Amplifier. The logarithmic amplifier has an input dynamic range of -200μV to -2 V, 3 nanosecond risetime, and an output of -.5 to +.6 volts [Ref. 13]. The logarithmic amplifier would compress the dynamic range of the return signal since it would only amplify the weaker signals. As the range increases the signal strength decreases and the amplification by the logarithmic amplifier increases.

The ground loop problem was corrected by making insulating sleeves for the bolts that fasten the receiver assembly to the mounting bracket and by the use of insulating spacers and washers.

Table 4: R1913 PHOTOMULTIPLIER SPECIFICATIONS [Refs. 1 and 14]

Cathode Sensitivity	65 milliAmperes/Watt (420 nanometers) 55 milliAmperes/Watt (532 nanometers)
Current Amplification (Gain)	3.0×10^3
Rise Time	1.0 nanosecond (2000 VDC)
Anode Dark Current	Typical 0.05 nanoAmperes Maximum 0.5 nanoAmperes
Spectral Response	Range 185-900 nanometers Peak Wavelength 420 nanometers
Quantum Efficiency	Average in the Visible Region 13% At 532 nanometers 15%

The use of a PMT, pre-amplifier, and a logarithmic amplifier required several different voltages to supplied. The voltages required were ± 5 V, ± 6V, +12 V, and - 18 V. Since a power supply that could supply all the required voltages does not exist commercially, one was designed and built (see Figure 10).

E. DATA ACQUISITION

The data collection was initially performed using the Hewlett Packard HP5411D Digitizing Oscilloscope which has a sampling rate of 1gigasample per second. Hard copies of the data were taken using a dot matrix printer and then scanning the displays for inclusion in this thesis. Additional data was collected using the Tektronix DSA 602A. The primary reason for shifting to the Tektronix was the increased ease of data storage since the DSA 602A has a built in disk drive. The DSA 602A also has a 2 gigasample per second sampling ability which could provide a better range resolution of the display. [Ref. 15]

The next chapter will present actual data taken and a discussion of the maximum clear air lidar return and hard target ranges.

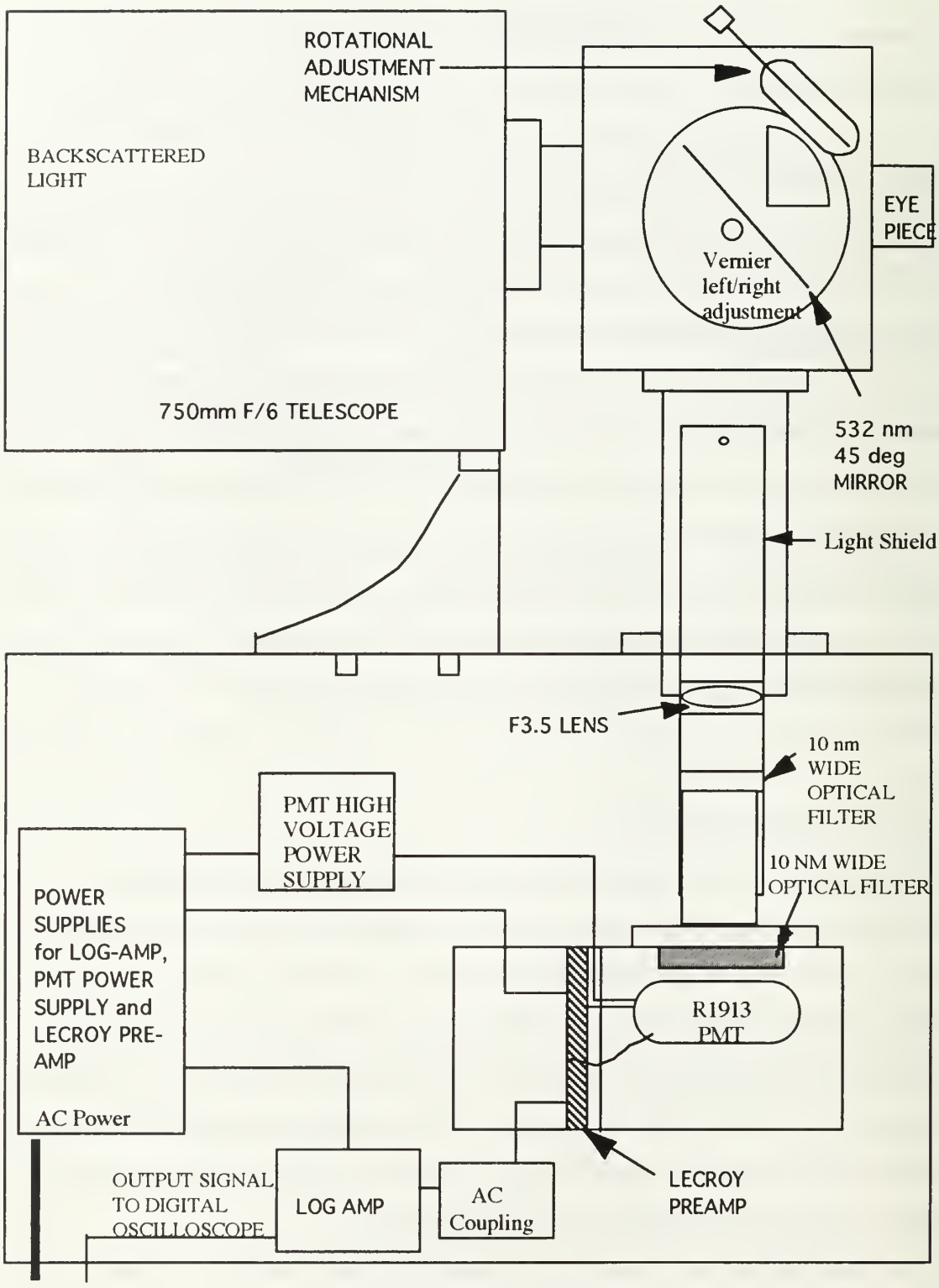

Figure 8. Receiver System.

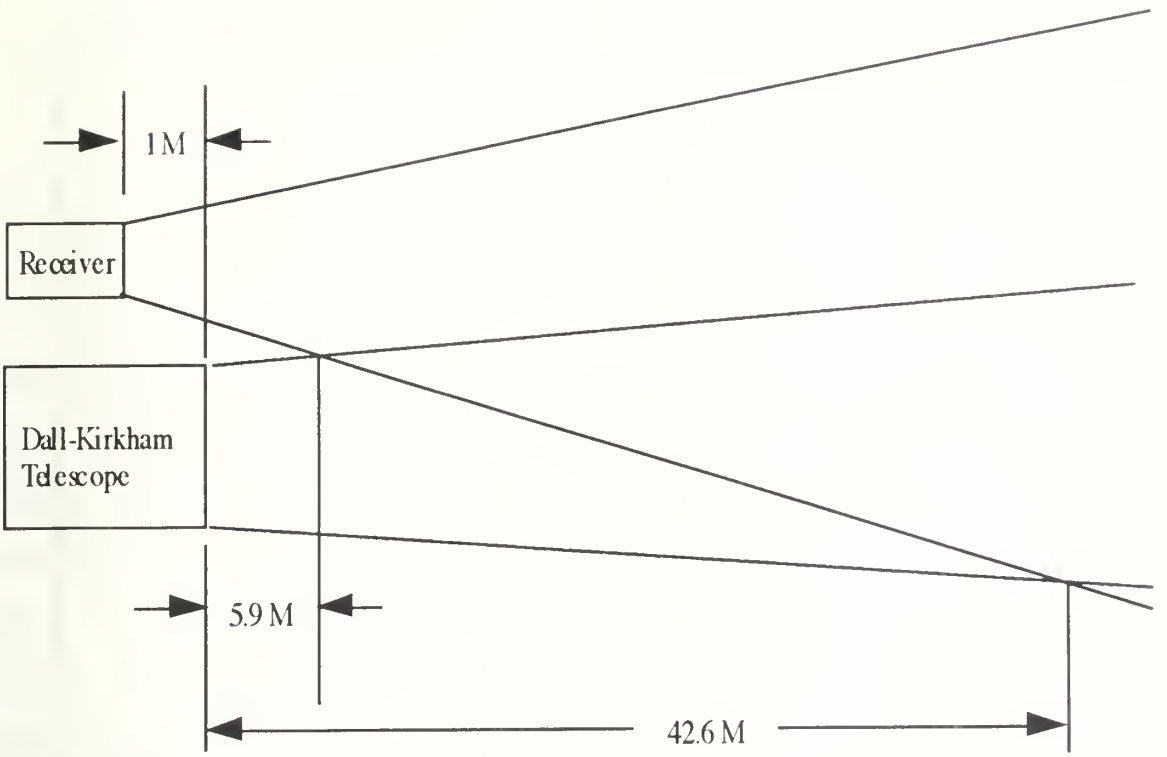

Figure 9. Graphical Solution for Beam Overlap.

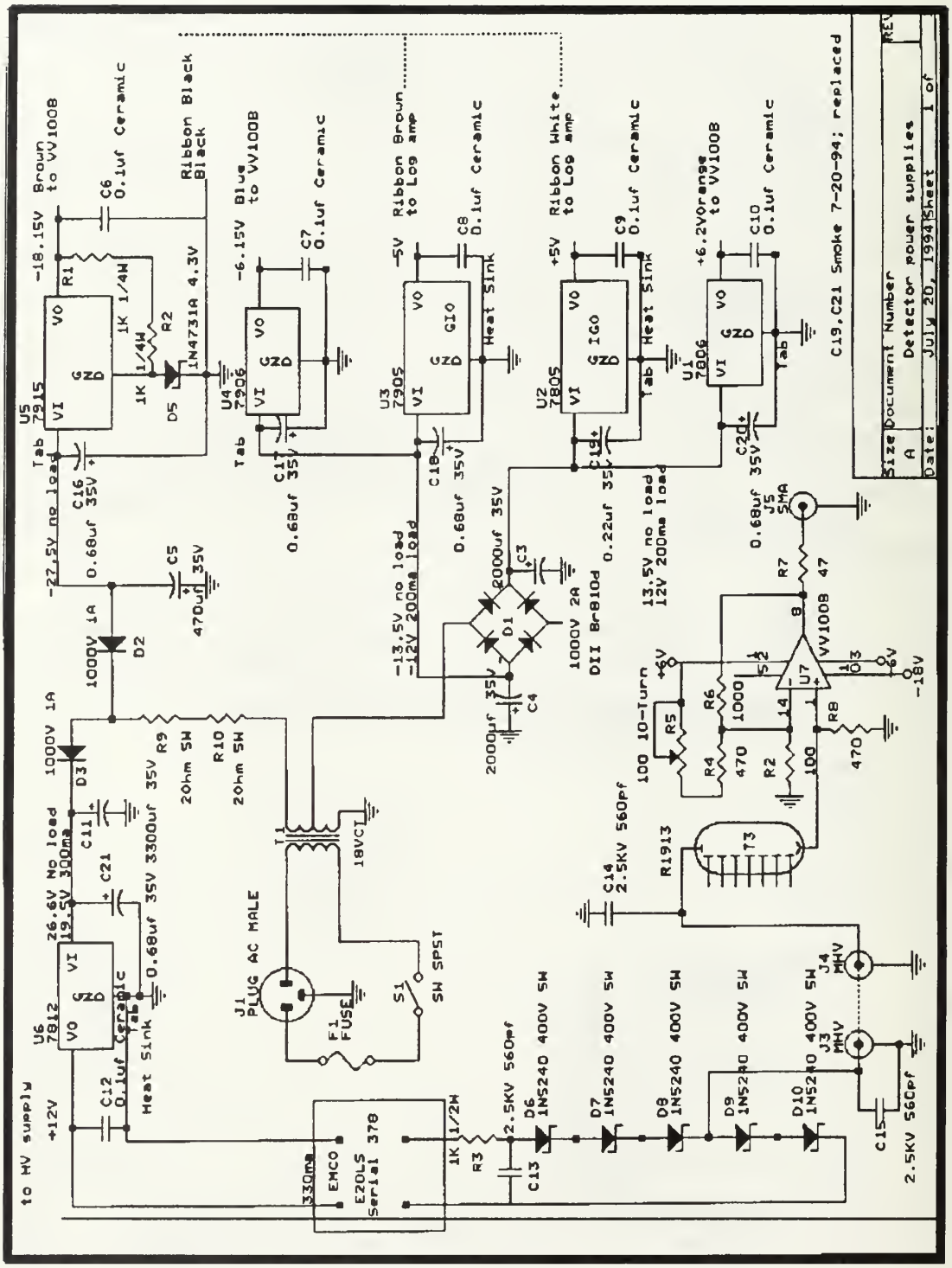

Figure 10. Detector System Power Supply.

IV. DATA COLLECTION AND ANALYSIS

A. SYSTEM DEMONSTRATION

The modified lidar system was tested on 2 August 1994 at 1430 hours to ensure that it was able to see clear air lidar signals. The system was pointed at a distant cloud bank and Figure 11 shows a strong lidar return out to a distance of 750 meters. This was before the system alignment was completed, with the High Voltage set at 1000 Volts and no logarithmic amplifier. The system demonstrated that atmospheric profiles can be monitored with the modified system. The weather was clear with a cloud bank moving in from the seaward side of Monterey. The lidar system was operated by the Physics Department staff initially and then the author took data with the Tektronix DSA 602A Digitizing Signal Analyzer described in Chapter III. The author had completed the required laser training to allow the operation of the system. The primary purpose of the test was to verify that the system could now be used to obtain lidar profiles of the atmosphere. The ultimate test is to determine if the lidar system is capable of good lidar returns of the boundary layer. To test the system several returns were taken and a selection of these are displayed in Figures 12 - 14.

B. RANGE LIMITS

There are two range limits that apply to the lidar system. The first is the maximum range for atmospheric monitoring. The second the maximum range to hard targets such as small hemispherical reflectors. The first limit is divided into daytime and night time maximum ranges.

The maximum theoretical daytime atmospheric lidar range can be determined

from Equation 2-14, using typical values for the atmospheric conditions and system parameters. The theoretical maximum daytime range is:

$$r_{max} = \sqrt{\frac{P_0 \tau \beta (r) \sqrt{c A_0 \lambda \eta (\lambda)} exp\left[-2\int_0^{r_{max}} \sigma (r')\, dr'\right]}{\sqrt{8h\Delta\lambda S_b (\lambda) \tau_0 (\lambda) \Omega_0 \Delta f}}} \qquad 4\text{-}1$$

where

r_{max} is the maximum range of the lidar system (meters),
P_0 is the transmitted power (0.4 x 10^6 watts, 2millijoules/5 nanoseconds),
τ is the laser pulse width (5 nanoseconds),
$\beta(r)$ is the atmospheric volume backscattering coefficient at range r (the values vary between 1 x 10^{-7} and 1 x 10^{-3} meters^{-1} * steradians^{-1} [Ref. 16]. A value of 1 x 10^{-5} will be used [Ref. 16]),
c is the speed of light (3 x 10^8 meters per second),
A_0 is the effective aperture of the receiver (0.113 meters^2),
λ is the wavelength of the background radiation which due to the narrow band filter can be assumed to be the same as the laser wavelength (532 x 10^{-9} meters),
$\eta(\lambda)$ is the quantum efficiency of the photomultiplier tube (15%),
$\sigma(r)$ is the atmospheric extinction coefficient (the values vary between 8 x 10^{-6} and 2 x 10^{-3} [Ref.17]. A value of 5 x 10^{-4} will be used),
h is Plank's constant (6.626176 x 10^{-34} watts * seconds^2),
$\Delta\lambda$ is the narrow band filter width (0.01 microns),
$S_b(\lambda)$ is the spectral radiance of the background (20 watts * meters^{-1} * steradians^{-1} * microns^{-1} [Ref. 6]),
$\tau_0(\lambda)$ is the receiver optics transmission efficiency at wavelength λ(0.25 due to the use of two 532 nm filters in series),
Ω_0 is the receiver solid angle (0.506 x 10^{-3} steradians), and
Δf is the receiver bandwidth (1 x 10^9 Hertz).

The resulting equation is:

$$r_{max} = 947.76 exp\left[-5 \times 10^{-4} r_{max}\right] \qquad \text{(meters)} \qquad 4\text{-}2$$

and must be solved numerically. The resulting maximum range is 676 meters.

For night time the theoretical maximum range is given by:

$$r_{max} = \sqrt{\frac{P_0 \tau \beta(r)\, \tau_0(\lambda)\, A_0 \lambda \eta(\lambda) exp\left[-2\int_0^{r_{max}} \sigma(r')\, dr'\right]}{4h\Delta f}} \quad . \qquad 4\text{-}3$$

Substituting the the known parameters into Equation 4-3 yields:

$$r_{max} = 1304 exp\left[-5 \times 10^{-4} r_{max}\right] \qquad \text{(meters)}. \qquad 4\text{-}4$$

Again the solution is found numerically and is 852 meters.

The maximum theoretical ranges will be compared to the actual lidar ranges obtained for daytime. Sufficient time was not available to allow recording of night time data.

The first lidar return was in good agreement with the expected daytime maximum range. However this was at a lower High voltage than the optimum. When an average of several shots is performed the range increases as expected.

The time scale in Figure 11 is 5 μseconds per centimeter. The return was the first strong clear lidar return and the system had not been aligned to fully maximize

.

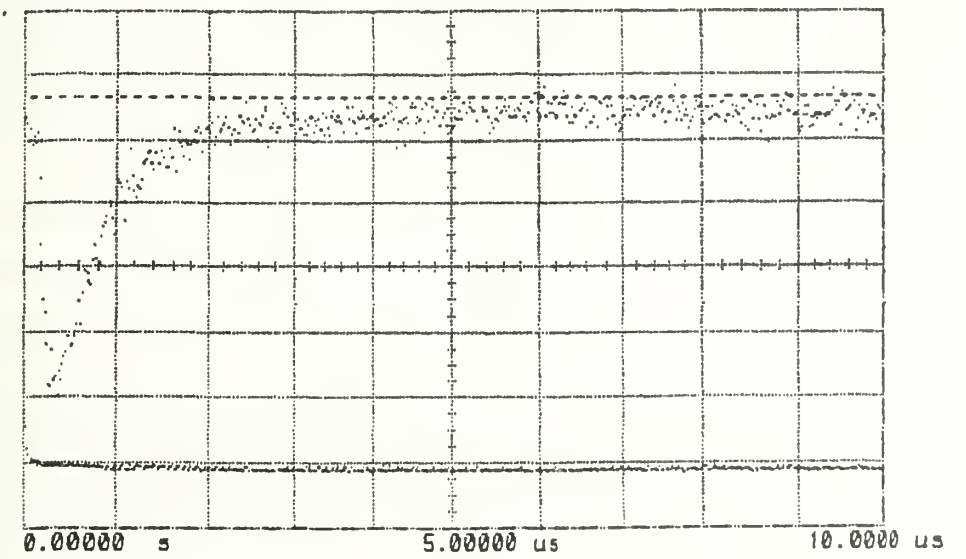

Figure 11. Clear air lidar return

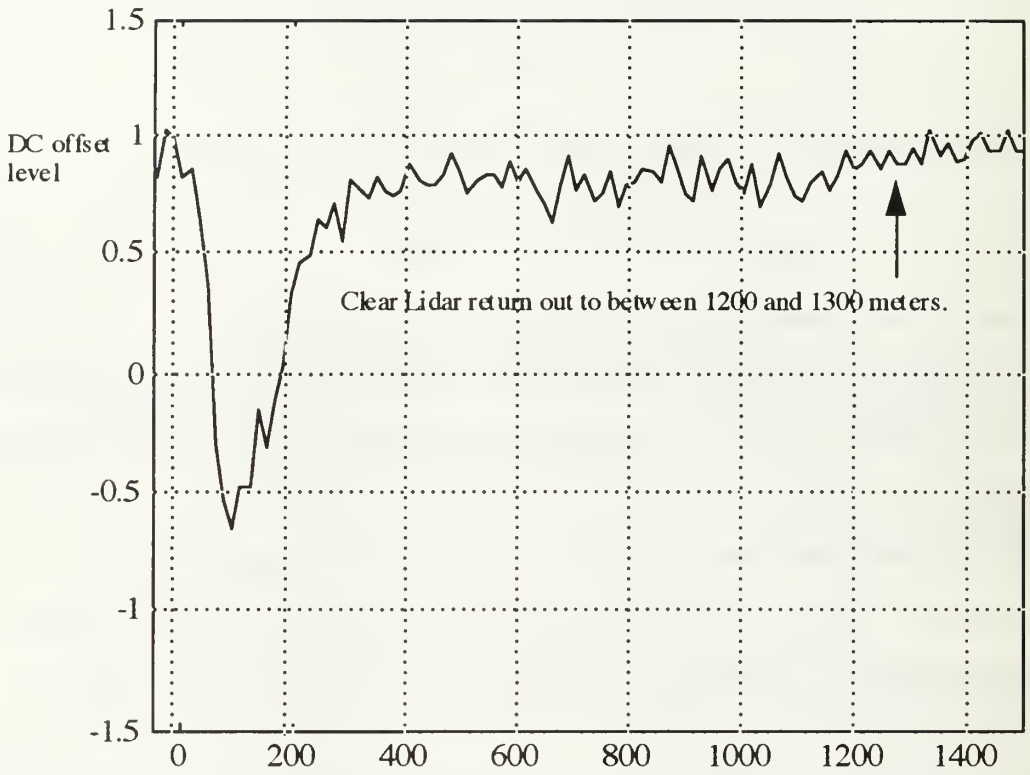

Figure 12. Clear Lidar Return After System Alignment Completed.

the signal. After the system alignment was completed clear returns were seen out to between 1200 and 1300 meters (see Figures 12 through 14).

The range can be increased by increasing the High Voltage to 1200 or 1600 volts. The SNR can be enhanced by averaging over several shots since the improvement is proportional to the square root of the number of samples [Ref. 6]. For example 16 shots results in an increase in the theoretical maximum range during daytime to approximately 2600 meters and for night time to approximately 8200 meters.

For hard target ranges the target reflectance and cross sectional areas must be known or a reasonable estimate made. The range equation for hard targets is given as: [Ref. 18]

$$r = \left[\frac{K P_0 \Gamma D^2 \eta_t \eta_r}{4\pi \varphi^2 P_r} \right]^{\frac{1}{4}} \qquad 4\text{-}5$$

where

K is the beam profile function,
P_0 is the transmitted power (watts),
Γ is the target laser cross section (meters^2),
D^2 is the receiver aperture diameter (meters),
η_τ is the transmitter optical efficiency,
η_r is the receiver optical efficiency,
φ is the laser beam width (radians), and
P_r is the received signal power (watts).

The beam profile for Gaussian beam is given by:

$$K(\psi, \varphi) = 2exp\left(\frac{-2r^2\psi^2}{\omega^2}\right) \qquad 4\text{-}6$$

where

φ is the laser beam width (radians),
ψ is the line of sight pointing error (radians).
r is the range to the target, and
ω is the Gaussian waist radius.

The target laser cross section for a sphere is given by: [Ref. 18]

$$\Gamma = \pi \rho z^2 \qquad 4\text{-}7$$

where

Γ is the target laser cross section (meters^2),
ρ is the reflectance of the sphere's surface, and
z is the radius of the sphere (meters).

For the NPS lidar system an estimate of a hard target maximum range is made using the following assumptions:

1. The hemispherical reflectance is 0.191 [Ref. 18].
2. The targets radius is 0.254 meters.
3. The pointing error is 1 milliradian (assumed value).

4. The receiver optical efficiency is 25%.
5. The beam profile function value is assumed to be 4, which is the value for a uniform beam and is more conservative than for a Gaussian beam [Ref. 18].
6. The transmitter optical efficiency is 60%.

Solving for the daytime maximum range yields 4700 meters. If the laser power were to be increased to 9 millijoules the maximum daytime range would be 6850 meters which is still less than the required 15 kilometers for integration into the IRST system. To meet this requirement would require an output power of 320 millijoules. This would result in a NHOD of 8530 meters. This could be a significant problem to friendly forces.

Possible improvements are:

1. Be able to change the field of view of the receiver depending on the range of interest. Hard target and atmospheric monitoring are the two cases of concern.
2. Remove the second filter when using the reduced field of view.

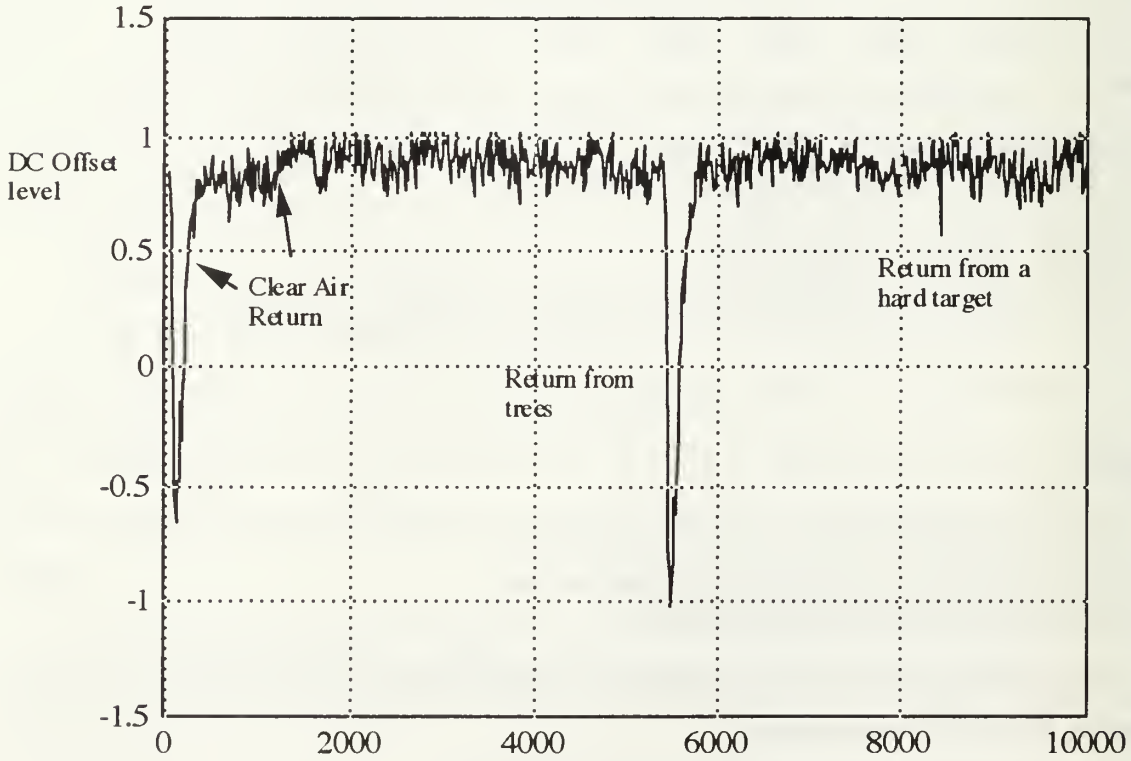

Figure 13. Lidar and Hard Target Returns.

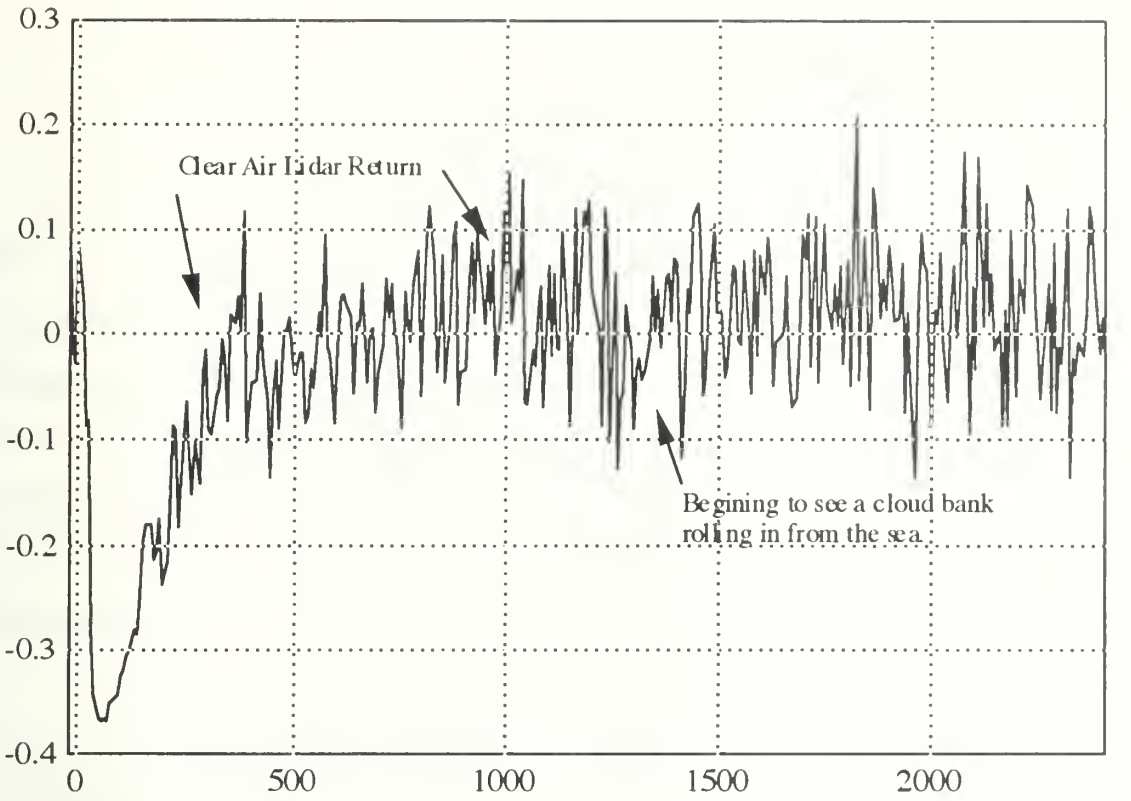

Figure 14. Lidar return and the edge of a cloud bank rolling in from sea.

The next chapter discusses the conclusions and recommendations for future work.

V. CONCLUSIONS AND RECOMENDATIONS

The current performance level of the telescope falls somewhat short of the requirement for a small, unattended, monitor of atmospheric profile stability. Trade offs may be made in the design, but the eye safety and range requirements necessitate a large optics transmitting aperture, dominating the size of the system. The NPS Lidar System was modified to enable the monitoring of the atmospheric marine boundary layer. The improvements in the system are:

1. The detector is now able to operate during daytime and provide the needed range to allow the boundary layer monitoring.
2. The shorter range for beam overlap allows the monitoring of the boundary layer from approximately 5.5 meters to 1.5 kilometers.
3. The installation of a beam expander in the transmitter has eliminated the problem of burning mirrors and made it easier to prevent the over filling of the mirrors in the transmitter telescope.
4. The alignment of the laser beam has been made significantly easier.
5. The ground loop problem was eliminated.
6. The trigger signal is much larger and very reliable.

There are more improvements that could be made in the future. Some of these are:

1. The mounting of the detector to the telescope needs to be modified to allow a more precise left/right and up/down adjustment.
2. A larger aperture telescope could be used on the receiver system to increase the ranges.
3. A new transmitter telescope could be used to improve the transmitter optical efficiency.

4. A method of attenuating the energy that is blocked by the secondary mirror needs to be developed.
5. The pan and tilt head assembly needs to be modified to allow the mounting bolts to clear the top of the cover when in the full vertical position.

Overall the system appears to be capable of use to monitor changes in the atmospheric marine boundary layer. As can be seen from the figures in Chapter IV the system can achieve clear air lidar returns out to the required distance of 1 kilometer. Once the pan tilt head is modified an actual vertical profile can be obtained and the atmospheric structure should be detectable. It should prove to be a good cuing device as to when a new radiosonde balloon launch is indeed necessary. The system is now capable of collecting the needed data to perform the comparison of radiosonde balloon profiles to lidar profiles.

This thesis has been a challenging and rewarding experience in lidar design. It has given the author a better understanding of the problems associated with the research and design of a system.

LIST OF REFERENCES

1. Regush, M.M., *Development of a LIDAR for Integration with the Naval Postgraduate School Infrared Search and Target Designation (NPS-IRSTD) System*, Master's Thesis, Naval Postgraduate School, Monterey, California, June 1993.

2. Measures, R.M., "Atmosphere Lidar Applications" in *Laser Remote Sensing Fundamentals and Applications*, pp. 320-413, Krieger Publishing Company, Malabar, Florida, 1992.

3. Measures, R.M., "Laser-Remote-Sensor Equations" in *Laser Remote Sensing Fundamentals and Applications*, pp. 237-280, Krieger Publishing Company, Malabar, Florida, 1992.

4. Harms, J.,"*Lidar return signals for coaxial and noncoaxial systems with central obstruction*" in Applied Optics, Vol. 18, No. 10, May 1979.

5. Price, W. J., "Photomultiplier Tubes" in *Nuclear Radiation Detection,* pp 174-178, McGraw-Hill Book Company, New York City, New York, 1964.

6. Measures, R.M., "Laser Systems as Remote Sensors" in *Laser Remote Sensing Fundamentals and Applications*, pp. 205-236, Krieger Publishing Company, Malabar, Florida, 1992.

7. Cooper, A. W., Lecture notes from PH3208, Electro-Optic Principles and Devices.

8. Davidson, K., Lecture notes from MR2416, Meteorology for Electronic Warfare.

9. Wallace, J. M. and Hobbs, P. V.,"Atmospheric Thermodynamics" in *Atmospheric Science An Introductory Survey*, pp. 47-51, Academic Press Inc., New York, New York, 1977.

10. American National Standards Institute, *American National Standard for Safe Use of Lasers*, ANSI Z136.1-1993, The Laser Institute of America, Orlando, Florida, 1993.

11. Cooper, A. W., Lecture notes from PH2207, Fundamentals Electro-Optics.

12. LeCroy Corporation, Model VV100B Wideband Pulse Amplifier Specifications, June 1988.

13. Analog Modules Inc., Model 382 Logarithmic Amplifier Specifications, February 1994.

14. Hamamatsu Corporation, *Photomultiplier Tube Catalog*, 1990.

15. Tektronix, *DSA602A Digitizing Signal Analyzer Users Manual*, 1992.

16. Measures, R.M., "Electromagnetic Theory of Radiation" in *Laser Remote Sensing Fundamentals and Applications*, pp. 11-58, Krieger Publishing Company, Malabar, Florida, 1992.

17. Measures, R.M., "Interaction and Propagation of Radiation" in *Laser Remote Sensing Fundamentals and Applications*, pp. 121-145, Krieger Publishing Company, Malabar, Florida, 1992.

18. Kamerman, G. W., "Laser Radar" in *The Infrared and Electo-Optical Systems Handbook*, pp. 2-35, v. 6, SPIE Optical Engineering Press, Bellingham, Washington, 1993.

INITIAL DISTRIBUTION LIST

1.	Defense Technical Information Center Cameron Station Alexandria, Virginia 22314-6145	2
2.	Library, Code 52 Naval Postgraduate School Monterey, California 93943-5101	2
3.	Chairman, Code EW Electronic Warfare Naval Postgraduate School Monterey, California 93943	1
4.	Professor A.W. Cooper, Code PH/Cr Department of Physics Naval Postgraduate School Monterey, California 93943	2
5.	Mr. W. Lentz, Code PH/Lz Department of Physics Naval Postgraduate School Monterey, California 93943	1
6.	Professor K. Davidson, Code MR/Ds Department of Meterology Naval Postgraduate School Monterey, California 93943	1
7.	Naval Command, Control and Ocean Surveillance Center NRad, Code 543 ATTN. Dr. D.R. Jensen, 271 Catalina Blvd, San Diego, CA 92152-5000	1
8.	Commander, Naval Sea Systems Command PMS - 400B ATTN: CDR J.W. Wilson Washington, DC 20363	1
9.	The Johns Hopkins University Applied Physics Laboratory Johns Hopkins Road Laurel, Maryland 20707 ATTN: Dr. M.J. Thomas, Code F1F	1

10. LCDR G. Mallo 1
1607 Rolling Ct. NW
Piedmount, Oklahoma 73078-9313

DUDLEY KNOX LIBRARY
NAVAL POSTGRADUATE SCHOOL
MONTEREY CA 93943-5101

DUDLEY KNOX LIBRARY
3 2768 00307949 2